Journal of Materials Chemistry A

ROYAL SOCIETY OF CHEMISTRY

COMMUNICATION

View Article Online
View Journal | View Issue

Cite this: J. Mater. Chem. A, 2020, 8, 13437

Received 28th March 2020
Accepted 24th June 2020

DOI: 10.1039/d0ta03470c

rsc.li/materials-a

Synergetic modulation of the electronic structure and hydrophilicity of nickel–iron hydroxide for efficient oxygen evolution by UV/ozone treatment†

Ying Pan,[a] Yanfang Wu,[b] H. Alex Hsain,[c] Ran Su,*[d] Claudio Cazorla[a] and Dewei Chu*[a]

In this work, a new surface engineering technique through UV/ozone treatment to improve the oxygen evolution reaction performance of nickel-iron hydroxide based catalysts has been developed. It is found that UV/ozone treatment can significantly improve the hydrophilicity of the catalysts as well as modify the electronic structure at the Ni–Fe center and oxidize Ni^{2+} to Ni^{3+}, which consequently enables better electrode–electrolyte contacts, stronger charge-transfer and more numbers of active sites with higher intrinsic activity during the OER. This work demonstrates UV/ozone treatment as a highly effective strategy towards the rational design of high-performance electrocatalysts by exploiting surface modifications.

Introduction

Water-splitting is one of the most advanced technologies to convert electricity to clean and sustainable hydrogen energy.[1] Optimizing a water-splitting system requires the development of highly efficient, low-cost and stable electrocatalysts.[2] Noble-metal-based electrocatalysts like RuO_2 and IrO_2 exhibit excellent electrocatalytic efficiency, however, the scarcity and high cost have largely impeded their practical application.[3] Therefore, high-performance electrocatalysts based on earth-abundant materials, especially for the oxygen evolution reaction (OER) which are bottlenecked by their sluggish kinetics in water splitting, are highly sought after. Among the electrocatalysts reported, metal hydroxides have been regarded as promising catalysts for the OER because of easy fabrication, abundant active sites, and outstanding catalytic activity.[4,5] However, the unsatisfactory electrical conductivity and low charge transfer in metal hydroxides have been a major technological obstacle towards their industrial application.

Recently, considerable efforts have been devoted to improving the electrocatalytic performance of metal hydroxides for the OER. Plenty of studies published so far have concentrated on the rational design of electrocatalysts by hierarchical or heterogeneous structuring,[6,7] atomic modification,[8] and materials hybridization.[9] However, these approaches sometimes involve complicated or multiple synthesis steps. Surface engineering, on the other hand, is a simple and straightforward method that can be used to tune the electronic properties and modify the surface chemical states of electrocatalysts. For example, thermal treatment under a reducing or inert atmosphere[10] is widely used to control the degree of crystallization and the element valence of electrocatalysts; flame engraving,[11] plasma treatment[12] and chemical etching in reducing environments ($NaBH_4$ (ref. 13) and ethylene glycol (EG) in alkaline solution,[14] *etc.*) have been used to generate oxygen vacancies in oxygen-containing catalysts; phosphatization,[15] sulfurization[16,17] and nitridation[18] are generally utilized to achieve a surface or interlayer anion exchange in catalysts at a nanoscale. Nevertheless, most of these treatments are time/energy-consuming, high-cost, or even toxic and require advanced facilities.

As one of the most commonly used pre/post-treatment methods, treatment with ultraviolet (UV)/ozone technology has long been used merely for surface cleaning/alteration but its potential application in OER catalysts has been hitherto unexplored.[19,20] The combination of UV irradiation and a strong oxidation atmosphere can effectively remove the capping agents and contaminants as well as improve the surface hydrophilicity of various materials. More importantly, the re-oxidation effect on catalysts can be realized by UV/ozone treatment,[20,21] which tunes the electronic structure of the electrocatalytically active center in the catalysts and thus enhances the intrinsic activity of active sites. Among different hydroxides, nickel hydroxides or Ni–Fe hydroxides exhibit excellent electrocatalytic

[a]School of Materials Science and Engineering, University of New South Wales, 2052, Australia. E-mail: d.chu@unsw.edu.au

[b]School of Chemistry, University of New South Wales, 2052, Australia

[c]Materials Science and Engineering, North Carolina State University, 27695, USA

[d]College of Science, Hebei University of Science and Technology, 050018, China. E-mail: suranxida@163.com

† Electronic supplementary information (ESI) available. See DOI: 10.1039/d0ta03470c

performance[22] and the OER involves the oxidation of Ni^{2+} to NiOOH intermediates. In comparison with Ni^{2+}, the highly oxidative Ni^{3+} species are more active and preferable for the formation and the subsequent deprotonation of NiOOH,[23] which indicates that designing electrocatalysts with higher ratios of Ni^{3+}/Ni^{2+} will boost the OER performance.

Inspired by the above considerations, we herein report the utilization of UV/ozone treatment to improve the OER performances of catalysts by using Ni–Fe hydroxides and nickel hydroxides as two control samples. It is found that UV/ozone treatment can remarkably enhance the hydrophilicity of catalysts to significantly facilitate electrode–electrolyte contact during the OER and modulate the electronic structure of the Ni–Fe center to effectively boost the intrinsic activity of active sites. As a result, the UV/ozone treated Ni–Fe hydroxides (or nickel hydroxides) exhibit a profoundly reduced overpotential of 272 mV (or 404 mV) as compared to the catalysts without UV/ozone treatment (327 mV and 461 mV, respectively) at a current density of 30 mA cm^{-2}. The exceptional catalytic performance of UV/ozone treated catalysts enables the potential application of UV/ozone treatment in practical large-scale catalyst design.

Results and discussion

The synthesis and UV/ozone treatment of the catalysts are illustrated in Fig. 1. Firstly, Ni–OH and NiFe–OH were synthesized through a hydrothermal method. Secondly, the obtained Ni–OH and NiFe–OH were loaded onto carbon paper as the working electrodes. Finally, the working electrodes were treated with or without UV/ozone for 2 h before electrochemical testing. The morphologies of the catalysts are characterized by Scanning Electron Microscopy (SEM) and Transmission Electron Microscopy (TEM). As shown in Fig. 2a and S2,† Ni–OH shows a free-standing 2D nanosheet morphology with an atomic thickness of ~4 nm (Fig. S3a and b†). With Fe doping, the free-standing 2D nanosheet evolves from large flat nanosheets to small wrinkled nanoflowers (Fig. 2b and S4†) with smaller lateral sizes and an atomic thickness of less than 2 nm (Fig. S3c and d†). The changes in the nanosheet architecture result in an enlarged Brunauer–Emmett–Teller (BET) surface area (Fig. S5†), providing faster mass diffusion and creating more accessible catalytically active sites for the catalysts.[24] After UV/ozone

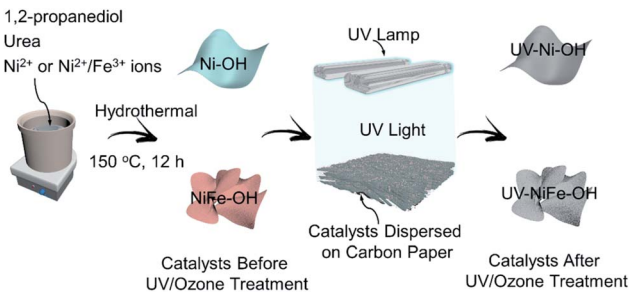

Fig. 1 Schematic illustration to show the synthesis of metal hydroxides and the process of UV/ozone treatment.

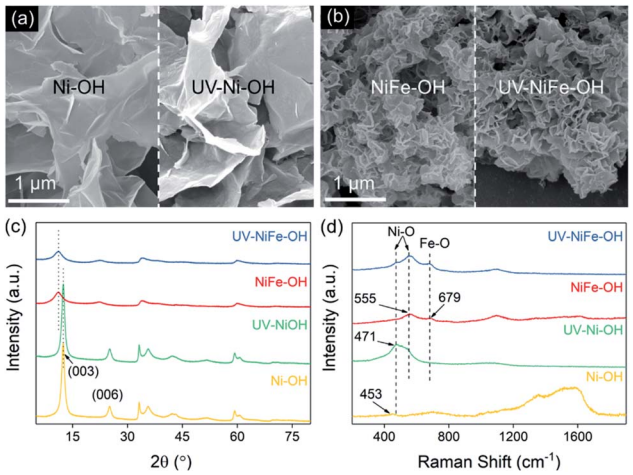

Fig. 2 SEM images of (a) Ni–OH and NiFe–OH. (b) UV–Ni–OH and UV–NiFe–OH. (c) XRD patterns and (d) Raman spectra of the catalysts.

treatment, the morphologies of UV–Ni–OH (Fig. 2a) and UV–NiFe–OH (Fig. 2b) show no obvious change as compared to those of Ni–OH and NiFe–OH, respectively.

The phase structures of the catalysts were characterized by X-ray diffraction (XRD). As shown in Fig. 2c, the diffraction pattern for Ni–OH matches well with α-$Ni(OH)_2$ (JCPDS: 38-0715) and β-$Ni(OH)_2$ (JCPDS: 14-0117) mixed phases. The diffraction pattern for NiFe–OH shows strong reflections associated with mixed NiFe layered double hydroxides with peaks at 12° (003) and 25° (006) shifting to lower angles relative to that of Ni–OH. In addition, the diffraction pattern shows lower crystallinity for NiFe–OH compared to Ni–OH,[25] which can be expected to increase the structural defects.[5] After UV/ozone treatment the XRD patterns of UV–Ni–OH and UV–NiFe–OH are almost unchanged in comparison to their untreated counterparts. Raman spectra (Fig. 2d) were collected to confirm the chemical bonding of the catalysts. The band at 453 cm^{-1} is attributed to the Ni–O bands in the $Ni(OH)_2$ phase.[26] The band that appeared at 679 cm^{-1} for NiFe–OH and UV–NiFe–OH is attributed to the Fe–O bond.[27] The increased intensities of bands at 471 cm^{-1} and 555 cm^{-1} observed in UV–Ni–OH and UV–NiFe–OH are attributed to Ni–O vibrations in NiOOH.[26] The broad peak around 1200–1600 cm^{-1} shown in the Ni–OH sample can be assigned to the nitrate ions from the nitrate salt precursor and the second internal O–H bending mode of the intercalated H_2O.[28] The spectral features and their changes confirm that UV/ozone treatment leads to the oxidation from the Ni^{2+} valance state to Ni^{3+} and the formation of stronger polar groups (–OOH). This oxidation effect without affecting the morphology and bulk phase structure of the catalysts has been shown to exhibit a more favorable hydrophilicity and much higher OER activity.[27]

X-ray photoelectron spectroscopy (XPS) measurements were conducted to characterize the surface elemental composition and valence states of the catalysts (Fig. 3 and S6†). The Ni 2p spectra of the catalysts (Fig. 3a and d) are fitted to six peaks which can be assigned to Ni^{2+} (855.5 eV and 873.2 eV), Ni^{3+}

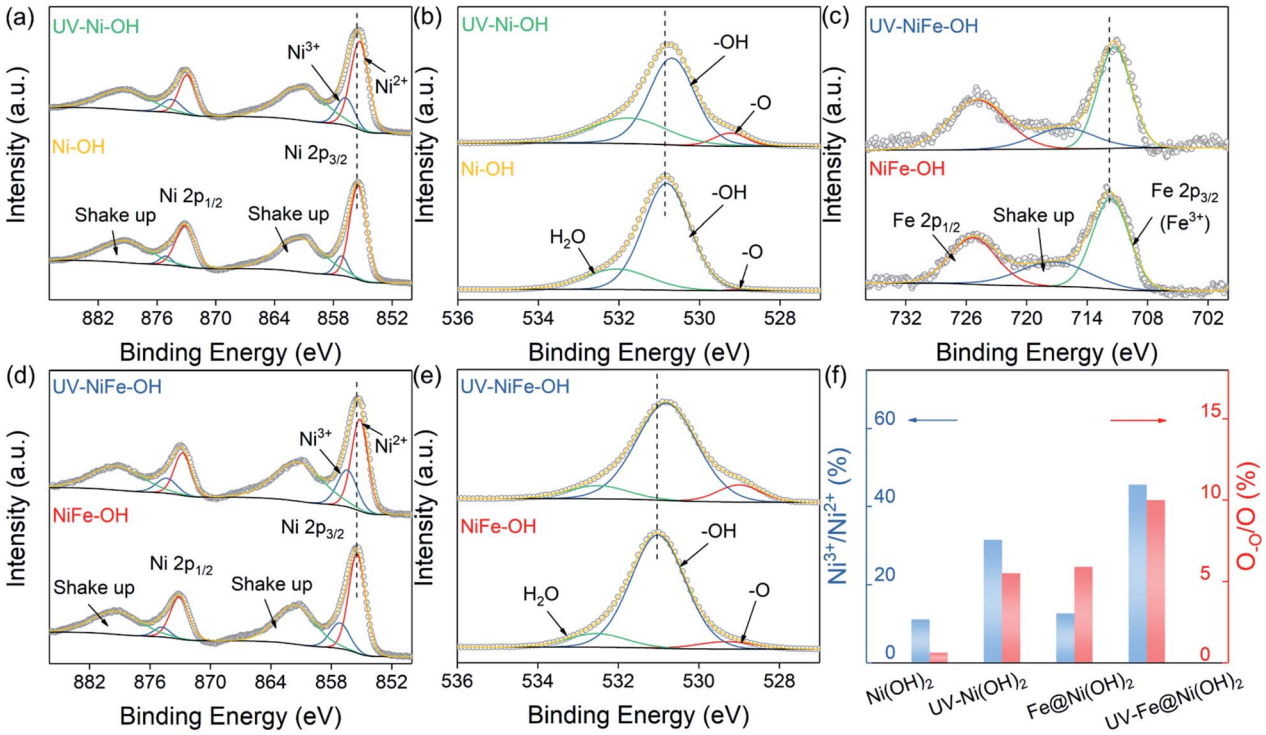

Fig. 3 High-resolution XPS spectra for the (a and d) Ni 2p, (b and e) O 1s and (c) Fe 2p regions of the catalysts. (f) Quantitative analysis of the XPS results of the catalysts.

(857.2 eV and 875.2 eV) and the corresponding shakeup (861.6 eV and 879.5 eV), respectively. The Ni^{3+} oxidation state in the Ni–OH sample may result from the aqueous solution processing and air exposure during drying processing.[29] The O 1s spectra of the catalysts (Fig. 3b and e) are well fitted into three peaks. The peaks centered at 530.8 eV and 532.1 eV are attributed to the metal hydroxyl (–OH) bond and the physisorbed/chemisorbed water (H_2O) on the surface, respectively.[30,31] The peak centered at 528.2 eV is attributed to the metal–oxygen(M–O) bond. The Fe spectra of NiFe–OH (Fig. 3c) show three peaks corresponding to Fe $2p_{3/2}$ (711.7 eV), Fe $2p_{1/2}$ (725.3 eV) and the shakeup (717.6 eV), respectively, which signifies the existence of iron in the Fe^{3+} valance state.[32] Compared to the XPS spectra of Ni–OH and NiFe–OH, significant red-shifts were observed for all the binding energies in the Ni 2p, O 1s and Fe 2p regions of UV–Ni–OH and UV–NiFe–OH XPS spectra, suggesting the presence of stronger electronic interactions among these components after UV/ozone treatment, expected to exert a positive effect on the catalytic activity of the catalysts.[33] Additionally, after UV/ozone treatment, Fe still exists as Fe^{3+} while the valence state of Ni changes. By quantifying the XPS spectra (Fig. 3f), it is clearly revealed that UV/ozone treatment increases the ratios of O_{-O}/O and Ni^{3+}/Ni^{2+} in UV–$Ni(OH)_2$ and UV–NiFe–OH relative to those in Ni–OH and NiFe–OH, respectively, further confirming its oxidizing effect.

To investigate the effects of UV/ozone treatment on the attachment characteristics of bubbles, the contact angles on the surface of catalysts were measured. As shown in Fig. 4, the contact angles of Ni–OH and NiFe–OH are both larger than 130°, showing their unfavorable hydrophobic feature. Fe doping might slightly increase the hydrophobicity of the catalyst due to its more hierarchical structure.[34] Once treated with UV/ozone, the contact angles of UV–Ni–OH and UV–NiFe–OH were both dramatically reduced to less than 15°. The results provide solid evidence of their ultrahigh hydrophilicity which will substantially increase the electrolyte–electrode contact points.[35]

The electrocatalytic performance of different samples was investigated by linear sweep voltammetry (LSV) in 1.0 KOH. Fig. 5a illustrates the *iR*-corrected polarization curves of the catalysts. Prior to water oxidation, Ni^{2+} $[Ni(OH)_2]$ → Ni^{3+}

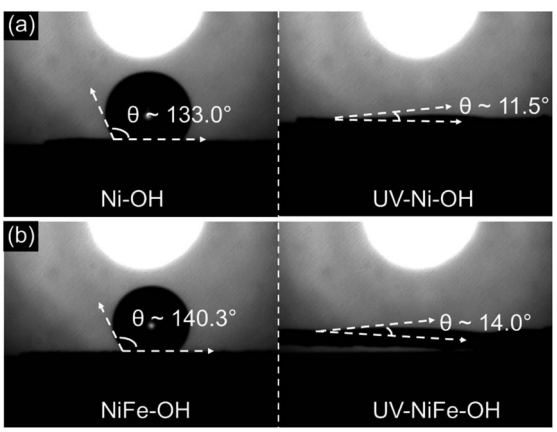

Fig. 4 Contact angles of (a) Ni–OH and UV–Ni–OH. (b) NiFe–OH and UV–NiFe–OH working electrodes.

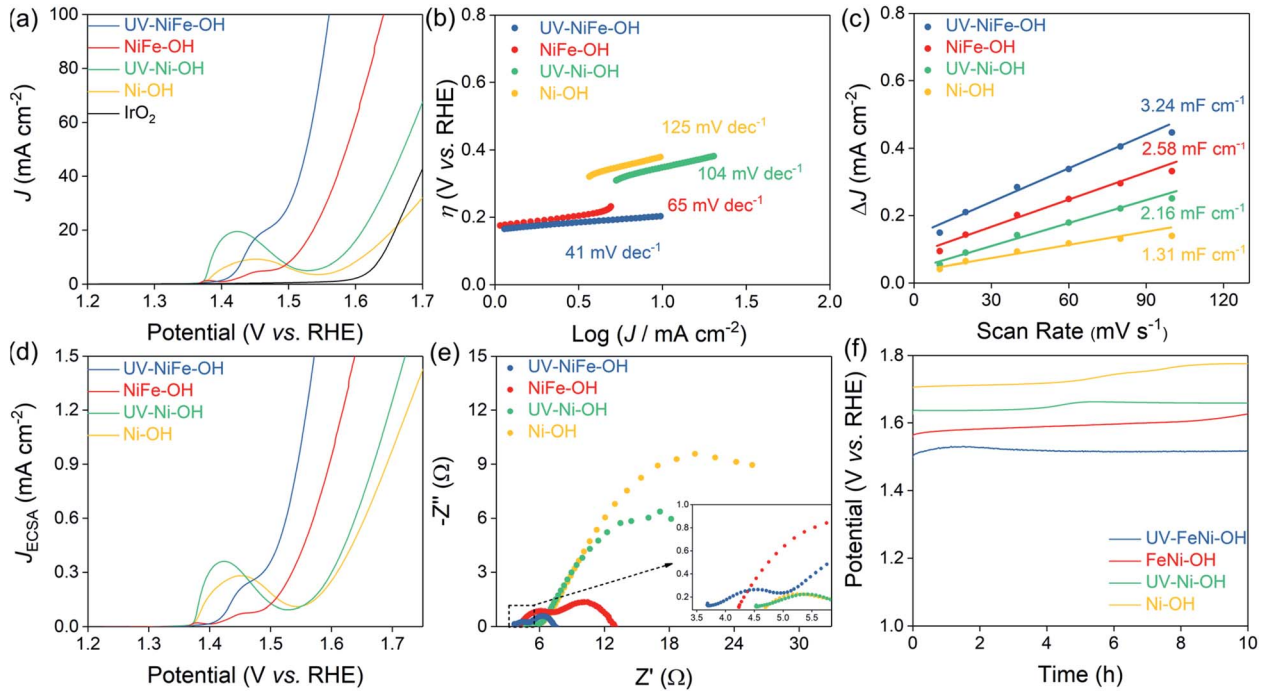

Fig. 5 (a) LSV curves of the catalysts for the OER with 90% *iR*-compensation at a scan rate of 5 mV s^{-1}. (b) Corresponding Tafel plots of the catalysts. (c) Double-layer capacitance (C_{dl}) as a function of the scan rate from CV curves. (d) LSV curves normalized by the ECSA from (a). (e) EIS results tested with a frequency from 0.1 Hz to 10 kHz. (f) Chronopotentiometry durability measurements at a constant current density of 30 mA cm^{-2}.

(NiOOH) redox transition can be found at ~1.4 V *vs.* RHE for Ni–OH. After Fe doping, the oxidation peak area of NiFe–OH decreases due to the depression effect of Fe^{3+} on the $Ni^{2+/3+}$ redox wave.[36] Upon treatment with UV/ozone, the oxidation peaks of UV–Ni–OH and UV–NiFe–OH slightly shift to lower potentials and the peak areas increase relative to Ni–OH and NiFe–OH, respectively, further implying the stronger electronic interactions in the catalysts due to the UV/ozone treatment as confirmed by XPS characterization. Notably, the overpotentials of UV–NiFe–OH at 30 mA cm^{-2} (η_{30}) and 50 mA cm^{-2} (η_{50}) are 272 mV and 297 mV, respectively, much superior to those of NiFe–OH ($\eta_{30} = 327$ mV and $\eta_{50} = 357$ mV) and commercial IrO_2 ($\eta_{30} = 448$ mV). UV/ozone treatment also has an evident effect on the OER kinetics of the catalysts, in which the Tafel slope (Fig. 5b) decreases from 65 mV dec^{-1} for NiFe–OH to 41 mV dec^{-1} for UV–NiFe–OH. The same positive effect is also revealed in the enhanced OER performance of the UV–Ni–OH catalyst compared to Ni–OH. Such remarkable performances also surpass those of reported $Ni(OH)_2$ materials to date (Table S1†). In addition, the LSV curves (Fig. S7†) were recorded for commercial IrO_2 and lab synthesized Co_3O_4 catalysts with/without UV/ozone treatment. The UV/ozone treated IrO_2 and Co_3O_4 both show higher current intensities than their counterparts, indicating that this UV/ozone treatment strategy can also be applied to some other transition metal-based catalysts.

To quantify the effective catalytically active sites in the catalysts, the electrochemical active surface areas (ECSAs, Table S2) are calculated from the electrochemical double-layer capacitance (C_{dl}) (Fig. 5c) extracted from CV plots (Fig. S8†). The ECSAs of UV–NiFe–OH and UV–Ni–OH are 81 and 54 cm^{-2}, much higher than those of NiFe–OH (64.5 cm^{-2}) and Ni–OH (32.7 cm^{-2}), respectively (Table S2†). The intrinsic activity of UV/ozone treated catalysts is also much higher than that of untreated ones as proven by the ECSA normalized LSV curves in Fig. 5d. Fig. 5e shows the electrochemical impedance spectroscopy (EIS) results. R_Ω (Fig. 5e inset) is the ohmic solution resistance, which is influenced by both the electrical conductivity of the electrolyte and the resistances in the working electrode.[37] R_{ct} is charge-transfer resistance and serves as a convenient index of the kinetic facility. The noticeable smaller semicircle radius (R_{ct}) (Fig. 5e) and internal resistance (R_Ω) (Fig. 5e: inset) of UV–NiFe–OH (or UV–Ni–OH) than NiFe–OH (or Ni–OH) indicates lower charge transfer resistance and better electrical conductivity for UV/ozone treated catalysts during the OER. The durability of the catalysts toward the OER was studied by the chronopotentiometry test (Fig. 5f). UV/ozone treated catalysts showed weaker fluctuations in potentials compared to Ni–OH and NiFe–OH in 10 h. Furthermore, electrodes after the chronopotentionmetry durability test were characterized by SEM, Raman and XPS to study the structural and chemical stability of the catalysts. No apparent morphology change is observed for UV treated samples (Fig. S9†), confirming the structural stability during the long-time reaction. The Raman (Fig. S10†) and XPS (Fig. S11 and 12†) spectra were almost the same as compared to those before the stability test (Fig. 2d and 3), suggesting no obvious change in the chemical bonding states for all samples. These results confirm the excellent

reproducibility and stability of UV/ozone treated catalysts toward the OER in strong alkaline media.

Based on the experimental results, a schematic model is proposed (Fig. 6 and S13†) and the remarkable OER performance of UV/ozone treated catalysts can be explained as follows: (i) for nickel hydroxide based catalysts, the OER proceed as $Ni(OH)_2 + OH^- \rightarrow NiOOH + H_2O + e^-$ in alkaline media. The $Ni^{3+/2+}$ provides the primary OER active sites, while Ni^{3+} is more active than Ni^{2+}. Increasing the ratio of Ni^{3+}/Ni^{2+} in the catalysts would then result in a better electrocatalytic activity. (ii) UV/ozone treatment is a photosensitized oxidation process, and oxygen will be dissociated to continuously generate and destruct ozone molecules as well as to create atomic oxygen by UV light according to the following two equations:[19]

$$2O_2 \xrightarrow{185\ nm} O_3 + O^*$$

$$O_3 \xrightarrow{254\ nm} O_2 + O^*$$

The highly reactive ozone molecules and atomic oxygen (O*) are strong oxidizing agents that may react with the metal ions to oxidize Ni^{2+} to Ni^{3+} as well as to alter the electronic structure of the Fe–Ni center. The number of active sites increases by virtue of the oxidation effect and the intrinsic activity of each active site increases because of the stronger electronic interactions at the Fe–Ni center, thus boosting the catalytic activity of the catalysts. Additionally, the altered electronic structure results in better conductivity and enhanced charge transfer of the catalysts during the OER. (iii) UV/ozone treatment not only removes the organic contaminants absorbed on the surface of the catalysts during the prolonged electrode preparation process but also modifies the surface properties, which tunes the wettability behavior of the catalysts from hydrophobic to hydrophilic. The high hydrophilicity guarantees much better catalyst–electrolyte interactions during the OER which are responsible for the increased OER activity.

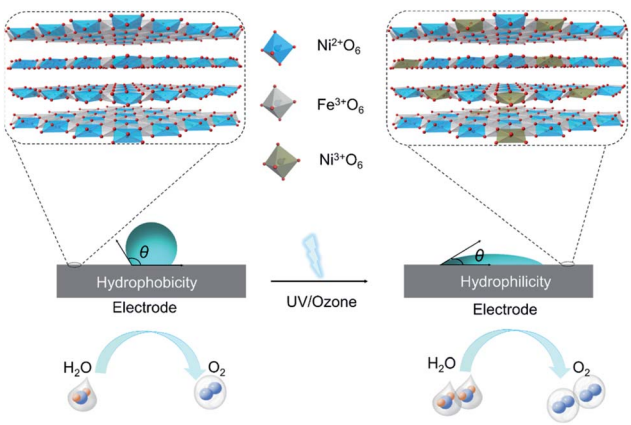

Fig. 6 Schematic illustration of the catalysts (left: NiFe–OH, right: UV–NiFe–OH) in the OER process.

Conclusions

In summary, we demonstrated the utilization of UV/ozone treatment as a facile approach to significantly improve the OER performance of electrocatalysts. The UV/ozone treated catalysts exhibit better catalytic activity and durability. UV/ozone treatment boosts the OER activity by providing highly reactive oxidizing agents; the atomic oxygen and ozone molecules, which modify the electronic structure of the Fe–Ni center, facilitate the oxidization of Ni^{2+} to Ni^{3+} and improve the hydrophilicity during the OER. These effects subsequently lead to decreased charge transfer resistance, increased electrical conductivity, the increased intrinsic activity of the active sites, the increased number/exposure of active sites and the significantly enhanced electrolyte–electrode contacts. This study is of great importance for opening a new dimension of efficient catalysts for water splitting by using cheap and easily handled preparation process.

Conflicts of interest

There are no conflicts to declare.

Acknowledgements

This work was funded by the Australian Research Council Project (grant no. FT140100032). Ying Pan thanks the China Scholarship Council (CSC) for financial support (no. 201604910910). H. Alex Hsain thanks the National Science Foundation Graduate Research Fellowship Program (DGE-1746939). The authors would like to thank Dr Haiwei Du at Anhui University, China for result discussion and manuscript revision.

References

1 I. Roger, M. A. Shipman and M. D. Symes, *Nat. Rev. Chem.*, 2017, **1**, 0003.
2 T. Wang, H. Xie, M. Chen, A. D'Aloia, J. Cho, G. Wu and Q. Li, *Nano Energy*, 2017, **1**, 69–89.
3 J. T. Ren, G. G. Yuan, C. C. Weng, L. Chen and Z. Y. Yuan, *Nanoscale*, 2018, **10**, 10620–10628.
4 J. Luo, J. H. Im, M. T. Mayer, M. Schreier, M. K. Nazeeruddin, N. G. Park, S. D. Tilley, H. J. Fan and M. Grätzel, *Science*, 2014, **345**, 1593–1596.
5 L. Trotochaud, S. L. Young, J. K. Ranney and S. W. Boettcher, *J. Am. Chem. Soc.*, 2014, **136**, 6744–6753.
6 B. M. Hunter, H. B. Gray and A. M. Muller, *Chem. Rev.*, 2016, **116**, 14120–14136.
7 S. Chen and S.-Z. Qiao, *ACS Nano*, 2013, **7**, 10190–10196.
8 W. Zhang, Y. Zou, H. Liu, S. Chen, X. Wang, H. Zhang, X. She and D. Yang, *Nano Energy*, 2019, **56**, 813–822.
9 Z. Xu, H. Pan, Y. Lin, Z. Yang, J. Wang and Y. Gong, *J. Mater. Chem. A*, 2018, **6**, 18641–18648.
10 N. Zhang, L. Cao, L. Feng, J. Huang, K. Kajiyoshi, C. Li, Q. Liu, D. Yang and J. He, *Nanoscale*, 2019, **11**, 11542–11549.

11 I. S. Cho, M. Logar, C. H. Lee, L. Cai, F. B. Prinz and X. Zheng, *Nano Lett.*, 2013, **14**, 24–31.
12 L. Xu, Q. Jiang, Z. Xiao, X. Li, J. Huo, S. Wang and L. Dai, *Angew. Chem., Int. Ed.*, 2016, **55**, 5277–5281.
13 L. Zhuang, L. Ge, Y. Yang, M. Li, Y. Jia, X. Yao and Z. Zhu, *Adv. Mater.*, 2017, **29**, 1606793.
14 Z. Cai, Y. Bi, E. Hu, W. Liu, N. Dwarica, Y. Tian, X. Li, Y. Kuang, Y. Li and X. Q. Yang, *Adv. Energy Mater.*, 2018, **8**, 1701694.
15 Q. Mo, W. Zhang, L. He, X. Yu and Q. Gao, *Appl. Catal., B*, 2019, **244**, 620–627.
16 S. Anantharaj, S. R. Ede, K. Sakthikumar, K. Karthick, S. Mishra and S. Kundu, *ACS Catal.*, 2016, **6**, 8069–8097.
17 Y. Pan, H. Ren, H. Du, F. Cao, Y. Jiang, H. Du and D. Chu, *J. Mater. Chem. A*, 2018, **6**, 22497–22502.
18 B. Liu, J. Cheng, H. Q. Peng, D. Chen, X. Cui, D. Shen, K. Zhang, T. Jiao, M. Li and C. S. Lee, *J. Mater. Chem. A*, 2019, **7**, 775–782.
19 J. R. Vig, *J. Vac. Sci. Technol., A*, 1985, **3**, 1027–1034.
20 R. Islam, G. Chen, P. Ramesh, J. Suh, N. Fuchigami, D. Lee, K. A. Littau, K. Weiner, R. T. Collins and K. C. Saraswat, *ACS Appl. Mater. Interfaces*, 2017, **9**, 17201–17207.
21 S. Huh, J. Park, Y. S. Kim, K. S. Kim, B. H. Hong and J.-M. Nam, *ACS Nano*, 2011, **5**, 9799–9806.
22 R. Subbaraman, D. Tripkovic, K. C. Chang, D. Strmcnik, A. P. Paulikas, P. Hirunsit, M. Chan, J. Greeley, V. Stamenkovic and N. M. Markovic, *Nat. Mater.*, 2012, **11**, 550–557.
23 O. Diaz-Morales, D. Ferrus-Suspedra and M. T. Koper, *Chem. Sci.*, 2016, **7**, 2639–2645.
24 Z. W. Seh, J. Kibsgaard, C. F. Dickens, I. Chorkendorff, J. K. Nørskov and T. F. Jaramillo, *Science*, 2017, **355**, eaad4998.
25 Y. Qiu, L. Xin and W. Li, *Langmuir*, 2014, **30**, 7893–7901.
26 J. Desilvestro, D. A. Corrigan and M. J. Weaver, *J. Am. Chem. Soc.*, 1988, **135**, 885–892.
27 M. W. Louie and A. T. Bell, *J. Am. Chem. Soc.*, 2013, **135**, 12329–12337.
28 D. S. Hall, D. J. Lockwood, C. Bock and B. R. MacDougall, *Proc. R. Soc. A*, 2015, **471**, 20140792.
29 H. Liu, Y. Wang, X. Lu, Y. Hu, G. Zhu, R. Chen, L. Ma, H. Zhu, Z. Tie and J. Liu, *Nano Energy*, 2017, **35**, 350–357.
30 X. Lu and C. Zhao, *Nat. Commun.*, 2015, **6**, 6616.
31 W. D. Chemelewski, H.-C. Lee, J.-F. Lin, A. J. Bard and C. B. Mullins, *J. Am. Chem. Soc.*, 2014, **136**, 2843–2850.
32 X. F. Lu, L. F. Gu, J. W. Wang, J. X. Wu, P. Q. Liao and G. R. Li, *Adv. Mater.*, 2017, **29**, 1604437.
33 Y.-F. Qi, Q. Wang, X.-G. Wang, Z.-Y. Liu, X.-J. Zhao and E.-C. Yang, *Nanoscale*, 2019, **11**, 10595–10602.
34 D. Quéré, *Annu. Rev. Mater. Res.*, 2008, **38**, 71–99.
35 J. Hao, W. Yang, Z. Huang and C. Zhang, *Adv. Mater. Interfaces*, 2016, **3**, 1600236.
36 M. Görlin, P. Chernev, J. Ferreira de Araújo, T. Reier, S. r. Dresp, B. Paul, R. Krähnert, H. Dau and P. Strasser, *J. Am. Chem. Soc.*, 2016, **138**, 5603–5614.
37 A. J. Bard, L. R. Faulkner, J. Leddy and C. G. Zoski, *Electrochemical Methods: Fundamentals and Applications*, Wiley, New York, 1980.

